Lattice relaxation at metal surfaces: An electrostatic model

Uzi Landman and Ross N. Hill
School of Physics, Georgia Institute of Technology, Atlanta, Georgia 30332

Mark Mostoller
Solid State Division, Oak Ridge National Laboratory, Oak Ridge, Tennessee 37830

(Received 30 August 1979)

Surface relaxation in metals is investigated via an electrostatic model, using an iterative scheme allowing for the participation of many layers in the relaxation process. Comparative studies of surface relaxation are performed for the low-index faces of Al, Li, Na, and Cu, using three models for the electronic density: (a) step function, (b) exponential, (c) Lang-Kohn. The results demonstrate the importance of multilayer relaxation mechanisms, and the sensititivy of the results to the model of the surface electronic density. For the exponential density profile, simple pseudopotential corrections are also included and shown to have significant effects. The relaxation trends predicted are consistent with available results obtained by analyses of low-energy-electron-diffraction data.

I. INTRODUCTION

Knowledge of the atomic arrangement in the surface region of metals is basic for the understanding of a large number of surface phenomena and interaction processes. This recognition has led to major efforts in the development of experimental and theoretical methods for the determination of surface structures.[1,2] The termination of a solid by a surface modifies both the atomic coordination and the conduction-electron distribution. In response, normal surface relaxation (deviations of distances between atomic planes from their bulk values) and surface reconstruction (lateral structural modifications) may occur. Surface relaxation has been observed[1] for a number of fcc, bcc, and hcp low-index clean metal surfaces and is the subject of the present investigation.

To elucidate the nature of the underlying forces which govern the surface crystallography, it is of interest to investigate surface structure theories of a predictive nature, which apart from their fundamental value could provide a source of model structures to employ in the analysis of experimental data. The first-principles determination of ionic positions at surfaces is hindered by difficulties in carrying out a self-consistent energy minimization for the coupled system of ions and conduction electrons. Semiempirical methods, on the other hand, which were developed originally mainly for the study of bulk defect configurations (pseudopotential pairwise interactions, empirically fitted pair potentials, and lattice statics methods) have usually predicted outward relaxations for low-index faces.[3-7] These results are in contradiction with experimental evidence indicating that contraction of the top interlayer spacing occurs in many if not most cases.

The inadequacies of surface relaxation models based on bulk-derived pair-potential interactions only have been emphasized by Finnis and Heine (FH).[8] Following the conclusion of Smoluchowski[9] (made in the context of a study of the work function) concerning the lateral smoothing of the electronic charge density at surfaces to lower the kinetic energy, FH presented a heuristic model of surface relaxation in *sp*-bonded materials. In this model the asymmetrical electron density at the cleaved surface is redistributed in surface Wigner-Seitz cells with a sharp cutoff at the solid-vacuum interface. As a result the ions at their first layer, truncated bulk positions experience a net electrostatic force to which they react via an inward relaxation. The original application of the model to the low-index faces of Al yielded results in qualitative agreement with experimental observations. Subsequent investigations have emphasized the importance of crystalline effects, as well as the influence of the inhomogeneous charge density distribution at the surface.[10] Most recently, a model which combined *ad hoc* short-range empirical pair interactions with forces on the first few layers arising from a step-function *sp*-electron density at the surface was employed to study the (100) face of α-Fe and Cu.[11]

To complement the above studies we describe here a simple electrostatic model for surface relaxation. The method combines the contribution to the force on ions in surface layers due to the delocalized valence electron distribution with that due to the interaction with the positive ionic charges in the planar nets. Three models for the electronic density in the surface region are studied and compared: (a) an abrupt terminated step density profile, (b) an exponential variational form (Smith),[12] and (c) a self-consistent distribution derived from the jellium model (Lang-Kohn).[13] For the exponential density profile, pseudopotential

corrections are also incorporated in a simple way. Under the influence of the forces acting on them, ions in an arbitrary number of surface planes are allowed to relax from their bulk positions, and the coupled set of equations governing the planar displacements are solved by a fast-converging iterative technique. The method is material dependent, in contrast to the original FH method. It is easy to apply and yields correct trends when compared with experimentally determined relaxation values for several materials. Following the derivation of the basic relations given in Sec. II, results obtained by the method are discussed in Sec. III.

II. EVALUATION OF THE SURFACE ELECTROSTATIC FORCES

In this section we derive expressions for the electrostatic interactions between ions in surface planes. For the sake of brevity we discuss first the case of a step-terminating electron density which is then generalized to the other density profiles considered. The arrangement of ions in the bulk terminated lattice is shown in Fig. 1(a): For simplicity, we consider only surfaces characterized by a single interlayer spacing d before relaxation. Ionic layers located at $-nd$ are embedded in slabs of thickness d and of uniform negative charge density $-(Ze/Ad)$, where Z is the valency of the material and A is the area of the unit cell of the surface net. The system after relaxation occurs is shown in Fig. 1(b).

The force on an ion in layer m due to the charge in a different layer n is evaluated by using a layer summation method.[11,14] The quantity of interest is the electrostatic potential at point r due to the charge in slab n:

$$\phi_n(\vec{r}) = \int \frac{\rho_n(\vec{r}')}{|\vec{r}-\vec{r}'|} d^3r' . \tag{1}$$

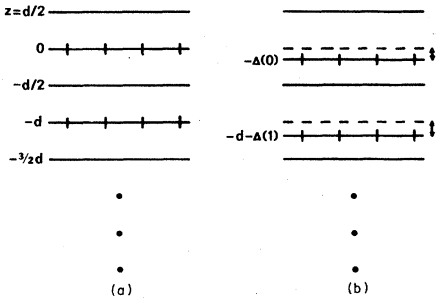

FIG. 1. Schematic picture of the layer arrangement in the terminated bulk crystal prior to (a) and after (b) relaxation. The bulk spacing is denoted by d and the displacement of ions in layer n from their bulk position by $\Delta(n)$.

Using the identity

$$\frac{1}{|\vec{r}-\vec{r}'|} = \frac{1}{2\pi}\int d^2K \frac{e^{-K|z-z'|}}{K} e^{i\vec{K}\cdot(\vec{R}-\vec{R}')}, \tag{2}$$

where $\vec{K}$ and $\vec{R}$ denote the projections of the vectors $\vec{k}$ and $\vec{r}$ onto the plane parallel to the surface plane, Eq. (1) can be written as

$$\phi_n(\vec{r}) = \frac{1}{2\pi}\int d^2K \frac{e^{\mp Kz}}{K} e^{i\vec{K}\cdot\vec{R}} \times \int d^3r' \rho_n(r') e^{\pm Kz'} e^{i\vec{K}\cdot\vec{R}'}; \quad z \gtrless z' . \tag{3}$$

Owing to the translational periodicity in the $2D$ net, the second integral in Eq. (3) can be written as

$$I = \frac{4\pi^2}{A}\sum_{\vec{G}} \delta(\vec{K}-\vec{G}) \int_{uc} d^3r' \rho_n(\vec{r}') e^{\pm Gz'} e^{-i\vec{G}\cdot\vec{R}'}, \tag{4}$$

where $\vec{G}$ is a reciprocal vector of the $2D$ net, and the integral remaining is over a neutral unit cell in slab n.

We now allow the ions in layer n to relax from their bulk position to a new location $z' = -[nd + \Delta(n)]$. Next we need to specify the layer-shift vectors defining the origins for the unit cells in the various layers. For the fcc (100) and (110) faces and the bcc (100) face, the layer shift vectors are

$$\vec{R}_n = \begin{cases} (0,0), & n \text{ even} \\ (a_1/2, a_2/2), & n \text{ odd}, \end{cases} \tag{5}$$

where a_1, a_2 are the magnitudes of the sides of the $2D$ unit cell; other cases are treated in Appendices A and B. Expressing the reciprocal lattice vector as $\vec{G} = \mu\vec{b}_1 + \nu\vec{b}_2$ (μ, ν integers), and introducing the function $P_{\vec{G}}(n)$ defined as

$$P_{\vec{G}}(n) \begin{cases} 1, & n \text{ even} \\ (-1)^{\mu+\nu}, & n \text{ odd}, \end{cases} \tag{6}$$

we obtain

$$I = \frac{4\pi^2}{A}(Ze) \sum_{\vec{G}}{}' \delta(\vec{K}-\vec{G}) P_{\vec{G}}(n) e^{\mp G[nd+\Delta(n)]}, \tag{7}$$

where the $-$ and $+$ signs correspond to the observation point $\vec{r}$ located above or below slab n, respectively. The prime on the sum in Eq. (7) indicates that the $\vec{G}=0$ term is excluded as a result of charge neutrality. Combining Eq. (7) with (3) yields for the z component of the electrostatic

field at $\vec{r}[E_z(\vec{r}) = -\partial\phi_n(\vec{r})/\partial z]$,

$$E_z(\vec{r}) = \pm\frac{2\pi}{A}(Ze)\sum_{\vec{G}}{}' e^{\mp Gz} e^{i\vec{G}\cdot\vec{R}} P_{\vec{G}}(n)\, e^{\mp G[nd+\Delta(n)]}. \quad (8)$$

Taking $z = -[md + \Delta(m)]$, and noting that $e^{i\vec{G}\cdot\vec{R}} = P^*_{\vec{G}}(m)$ for an ion in layer m, we find that the force on ions in layer m due to the charge in layer n is, in units of $2\pi(Ze)^2/A$,

$$F_{mn} = \mathrm{sgn}(n-m)\sum_{\vec{G}}{}' P^*_{\vec{G}}(m) P_{\vec{G}}(n) \exp[-G\,|\,(n-m)d + \Delta(n) - \Delta(m)\,|\,], \quad m \neq n. \quad (9)$$

The interaction of the ions in slab m with the negative charge in the same slab is obtained by using the Poisson equation, which yields for the z component of the force in the same units as above,

$$F_{mm} = 2\Delta(m)/d. \quad (10)$$

Let us assume that relaxation from bulk positions occurs up to layer L, i.e., for $n > L$, $\Delta(n) = 0$, and sum the contributions to the force on ions in layer m from these deep layers. The result is

$$F_m = \sum_{n=L+1}^{\infty} F_{mn} = \sum_{\vec{G}}{}' P^*_{\vec{G}}(m) e^{G[md+\Delta(m)]} \sum_{n=L+1}^{\infty} P_{\vec{G}}(n) e^{-Gdn}. \quad (11)$$

For two-layer repeat sequences in the $2D$ layer shift vectors as in Eq. (5), F_m is given by

$$F_m = \sum_{\vec{G}}{}' \frac{P_{\vec{G}}(L+1)e^{-Gd} + P_{\vec{G}}(L+2)e^{-2Gd}}{1 - e^{-2Gd}} P^*_{\vec{G}}(m)\, e^{-G[(L-m)d - \Delta(m)]}. \quad (12)$$

The simultaneous set of equations for static equilibrium is

$$0 = \sum_{n=0}^{L} F_{mn}(\Delta_m, \Delta_n) + F_m(\Delta_m) \quad \text{for } m = 0, 1, \ldots, L. \quad (13)$$

The solution of the above set of equations is achieved by a simple iterative method in which we set $\Delta_{i+1}(n) = \Delta_i(n) + \delta_i(n)$, where i is the iteration number. The procesure is started with $\Delta_1(n) = 0$ for all n. Expansion of the forces in Eq. (13) to first order in $\delta_i(n)$ yields the following set of equations:

$$\sum_{l'=0}^{L} a_{ll'}\delta_i(l') = b_l; \quad l = 0, 1, \ldots, L, \quad (14)$$

$$a_{ll'} = -\sum_{\vec{G}}{}' P^*_{\vec{G}}(l) P_{\vec{G}}(l') G \exp[-G\,|\,(l'-l)d + \Delta_i(l') - \Delta_i(l)\,|\,], \quad l \neq l', \quad (15a)$$

$$a_{ll} = \sum_{n\neq l}\sum_{\vec{G}}{}' P^*_{\vec{G}}(l) P_{\vec{G}}(n) G \exp[-G\,|\,(n-l)d + \Delta_i(n) - \Delta_i(l)\,|\,] + \sum_{\vec{G}}{}' \frac{P_{\vec{G}}(L+1)e^{-Gd} + P_{\vec{G}}(L+2)e^{-2Gd}}{1 - e^{-2Gd}} P^*_{\vec{G}}(l) G \exp\{-G[(L-l)d - \Delta_i(l)]\} + 2/d, \quad (15b)$$

$$b_l = -\sum_{n\neq L} \mathrm{sgn}(n-l) \sum_{\vec{G}}{}' P^*_{\vec{G}}(l) P_{\vec{G}}(n) \exp[-G\,|\,(n-l)d + \Delta_i(n) - \Delta_i(l)\,|\,] - \sum_{\vec{G}}{}' \frac{P_{\vec{G}}(L+1)e^{-Gd} + P_{\vec{G}}(L+2)e^{-2Gd}}{1 - e^{-2Gd}} P^*_{\vec{G}}(l) \exp[-G\,|\,(L-l)d - \Delta_i(l)\,|\,] - 2\Delta_i(l)/d. \quad (15c)$$

The values of $\delta_i(l)$ in each iteration are obtained from Eq. (14) by simple matrix inversion. Typically the solution converges after 3–5 iterations.

Exponential density profile

Having derived the basic relations for the step-terminating electronic distribution, we turn now to a generalization of the theory to include more realistic descriptions of the surface electron density profile. First we employ an exponential form.

$$\rho_e(z) = n_0\left(1 - \frac{e^{\beta(z-d/2)}}{2}\right), \quad z < \tfrac{1}{2}d \quad (16a)$$

$$\rho_e(z) = \tfrac{1}{2}n_0\, e^{-\beta(z-d/2)}, \quad z > \tfrac{1}{2}d \quad (16b)$$

where $n_0 = -Ze/Ad$ and β is a variational parameter.[12] Let us consider first the electronic field at a point z in the first layer. Integration of the Poisson equation yields

$$E_z(z) = 4\pi\int_{\infty}^{z} \rho_e(z')dz' + E_z(z\to\infty), \quad (17)$$

where $E_z(z\to\infty) \to 4\pi n_0 d/2$. Using Eqs. (16a) and (16b), we obtain

$$E_z(z) = 4\pi n_0\left[z - \frac{e^{\beta(z-d/2)}}{2\beta}\right]. \quad (18)$$

Setting $z=-\Delta(0)$, we find that the force on the first layer of ions due to the negative charge in the outermost region is, in units of $2\pi(Ze)^2/A$,

$$F_{00}=\frac{2}{d}\left(\Delta(0)+\frac{e^{-\beta[\Delta(0)+d/2]}}{2\beta}\right). \tag{19}$$

In the language of our iterative algorithm ($\Delta_{i+1}=\Delta_i+\delta_i$),

$$F_{00}=\frac{2}{d}\left(\Delta_i(0)+\frac{e^{-\beta[\Delta_i(0)+d/2]}}{2\beta}\right)+\frac{2}{d}\left(1-\frac{e^{-\beta[\Delta_i(0)+d/2]}}{2}\right)\delta_i(0). \tag{20}$$

Thus to b_0 in Eq. (15c) we need to add the factor $-(\beta d)^{-1}\exp\{-\beta[\Delta_i(0)+d/2]\}$ and to a_{00} in Eq. (15b) the factor $-d^{-1}\exp\{-\beta[\Delta_i(0)+d/2]\}$.

Next we consider the change in the force acting on ions in the second slab. Since we require a division of the material into neutral regions we need to adjust the location of the boundary between the outermost and the next region from its original position at $-d/2$ to $-d/2+s$. The shift in the boundary is determined by the condition $E(s-d/2)=-4\pi n_0 d/2$, or using Eq. (18),

$$2\beta s=e^{\beta(s-d)}. \tag{21}$$

The electric field in the second layer is given by

$$E_z(z)=4\pi\int_{-d/2+s}^{z}\rho(z)dz+E_z(z\to\infty). \tag{22}$$

Substituting Eq. (16a) in Eq. (23) and using Eq. (22), then setting $z=-[d+\Delta(1)]$ for the second layer and employing our iterative scheme, we obtain

$$F_{11}=\frac{2}{d}\left[\Delta_i(1)+\delta_i(1)+\frac{e^{-\beta[\Delta_i(1)+3d/2]}}{2}\left(\frac{1}{\beta}-\delta_i(1)\right)\right]. \tag{23}$$

Thus to b_1 in Eq. (15c) we need to add $-(\beta d)^{-1}\exp\{-\beta[\Delta_i(1)+3d/2]\}$ and to a_{11} in Eq. (15b) that term multiplied by β.

Lang-Kohn density profile

The importance of self-consistency in the calculation of a number of surface properties such as surface energies, work functions, adsorption, and geometrical structure has been investigated and demonstrated. Since the exponential density does not include some features characteristic of the electronic density at surfaces, such as Friedel oscillations, we employ next the self-consistent surface electronic density calculated by Lang and Kohn[13] (LK) for a uniform positive background model. These charge densities have been tabulated for various r_s values in Table I of Ref. 13 and will be denoted by n_{LK}. Using our previous notation, the z component of the electric field on ions in the first layer of the solid can be written as

$$\begin{aligned}E_z[-\Delta_i(0)-\delta_i(0)]&=E_z[-\Delta_i(0)]+4\pi n_{\mathrm{LK}}[-\Delta_i(0)]\delta_i(0)\\&=-4\pi\frac{Ze}{Ad}\int_{\infty}^{-\Delta_i(0)}n_{\mathrm{LK}}(z)dz-4\pi\frac{n_0Ze}{Ad}\frac{d}{2}\\&\quad-4\pi\frac{Ze}{Ad}n_{\mathrm{LK}}[-\Delta_i(0)]\delta_i(0),\end{aligned} \tag{24}$$

from which the force F_{00} follows. Accordingly the term $-2\Delta_i(0)/d$ in Eq. (15c) for b_0 is replaced by $(2/d)\int_{\infty}^{-\Delta_i(0)}n_{\mathrm{LK}}(z)dz+1$, and in Eq. (15b) for a_{00} the term $2/d$ is replaced by $(2/d)n_{\mathrm{LK}}[-\Delta_i(0)]$. To include effects on ions in the second layer the corresponding replacements in b_1 and a_{11} are made with the terms evaluated at $z=-[d+\Delta_i(1)]$. Notice also that due to a difference in the choice of origin for the location of the first layer of ions at the surface, the LK coordinates are shifted by $+d/2$ to agree with our convention.

Pseudopotential corrections

To incorporate pseudopotential corrections within the framework of our model, we use a simplified Heine-Abarenkov pseudopotential[15,16] for the electron-ion interaction. The difference from the Coulomb interaction used in Eq. (1) and subsequently is given by the function

$$f(|\vec{r}'-\vec{r}|)=\theta(r_0-|\vec{r}'-\vec{r}|)\left(\frac{1}{a_0}-\frac{1}{|\vec{r}'-\vec{r}|}\right), \tag{25}$$

where r_0 and a_0 are the pseudopotential radius and well-depth parameter, respectively, and θ is the Heaviside step function [$\theta(x)=1$, $x>0$ and $\theta(x)=0$, $x<0$]. For $a_0\to\infty$, the simplified Heine-Abarenkov pseudopotential becomes an Ashcroft pseudopotential.[17]

If the pseudopotential cores do not overlap, then the only change in the potential acting on an ion is that due to the difference of its own pseudopotential core from the Coulomb interaction,

$$\begin{aligned}\Delta\phi_n\{\vec{r}=-[nd+\Delta(n)]\hat{z}+\vec{R}]\}&=-\int d^3r'\rho_e(\vec{r}')f(|\vec{r}'-\vec{r}|)\\&=-2\pi\int_{-r_0}^{r_0}dz\,\rho_e\{z-[nd+\Delta(n)]\}\\&\quad\times\left(\frac{1}{2a_0}(r_0^2-z^2)-r_0+|z|\right).\end{aligned} \tag{26}$$

For a constant charge density ρ_0 across the pseudopotential core, the integral in Eq. (26) yields a constant potential,

$$\Delta\phi_n\{\vec{r}=-[nd+\Delta(n)]\hat{z}+\vec{R}\}=2\pi\rho_0r_0^2[1-\tfrac{2}{3}(r_0/a_0)], \tag{27}$$

and no change occurs in the forces exerted on the ion. However, when the planes of ions relax in regions of nonuniform electronic charge density, the pseudopotential corrections do modify the forces acting on the ions, as we illustrate for the exponential density profile.

We consider first the case, where $nd+\Delta(n)+d/2 > r_0$, and the exponential density to use in Eq. (26) is that given in Eq. (16a). Carrying through the integration in Eq. (26), we obtain

$$\Delta\phi_n\{\vec{r}=-[nd+\Delta(n)]\hat{z}+\vec{R}\}=2\pi n_0\left\{r_0^2[1-\tfrac{2}{3}(r_0/a_0)]-\frac{1}{\beta^2}e^{-\beta[nd+\Delta(n)+d/2]}\left([1-(r_0/a_0)]\coth\beta r_0+\frac{1}{\beta a_0}\sinh\beta r_0-1\right)\right\}. \tag{28}$$

The change in the force on an ion in plane n is $\Delta F_{nn}=d\Delta\phi_n/d\Delta(n)$, which in units of $2\pi(Ze)^2/A$ is

$$\Delta F_{nn}=\frac{1}{\beta d}e^{-\beta[nd+\Delta(n)+d/2]}\left([1-(r_0/a_0)]\coth\beta r_0+\frac{1}{\beta a_0}\sinh\beta r_0-1\right), \tag{29}$$

which for the Ashcroft pseudopotential ($a_0\to\infty$) reduces to

$$\Delta F_{nn}\to\frac{1}{\beta d}e^{-\beta[nd+\Delta(n)+d/2]}(\coth\beta r_0-1). \tag{30}$$

Note that this is the change relative to the results obtained for the exponential density profile with a Coulomb electron-ion interaction. The changes with respect to the step-function density profile results given in Eqs. (15a)–(15c) are

$$\begin{aligned}\delta a_{11}&=\beta\delta b_1\\&=-\frac{1}{d}e^{-\beta[nd+\Delta(n)+d/2]}\left([1-(r_0/a_0)]\coth\beta r_0+\frac{1}{\beta a_0}\sinh\beta r_0\right)\\&\xrightarrow[a_0\to\infty]{}-\frac{1}{d}e^{-\beta[nd+\Delta(n)+d/2]}\coth\beta r_0.\end{aligned} \tag{31}$$

If the pseudopotential core for an ion in the first layer intersects the plane at $d/2$, i.e., $\Delta(0)+d/2 < r_0$, the pseudopotential corrections are obtained by using both (16a) and (16b) for ρ_e in the appropriate ranges in the integral in Eq. (26). For this case, we will simply give expressions for the changes relative to the step function density results in Eqs. (15a)–(15c):

$$\delta a_{11}=\frac{1}{d}\left[\left(1-(r_0/a_0)-\frac{1}{\beta a_0}\right)e^{-\beta r_0}\sinh\{\beta[\Delta(0)+d/2]\}-1+\frac{1}{a_0}[\Delta(0)+d/2]\right], \tag{32a}$$

$$\begin{aligned}\delta b_1=-\frac{1}{\beta d}\Bigg[&\left(1-(r_0/a_0)-\frac{1}{\beta a_0}\right)e^{-\beta r_0}\\&\times\coth\{\beta[\Delta(0)+d/2]\}\\&+\frac{1}{\beta a_0}+\beta\{r_0-[\Delta(0)+d/2]\}\\&\times\left(1-\frac{1}{2a_0}[r_0+\Delta(0)+d/2]\right)\Bigg].\end{aligned} \tag{32b}$$

III. RESULTS

We have applied the methods described in the previous section to investigate relaxation at the low-index faces of several fcc and bcc materials. A summary of characteristic parameters for the (001), (110), and (111) faces of fcc and bcc crystals is given in Appendix B.

Several studies of electrostatic contributions to surface relaxation have been reported previously.[8,10,11] In all of these, it was concluded that the contribution of electrostatic forces arising from the smoothed sp-electron charge density is important, and cannot be neglected with respect to short-range forces and broken bonds which generally, by themselves, predict outward relaxations. No systematic investigation has yet been made, however, of the effects of physically reasonable variations within an electrostatic model. We will show that three such variations produce quantitatively significant effects: (1) multilayer relaxation, (2) charge density profiles, and (3) pseudopotential corrections.

Table I illustrates the importance of multilayer relaxation mechanisms for exponential charge density profiles at Al and Na surfaces with no pseudopotential corrections. Similar results are obtained with the step function and Lang-Kohn densities. The effect of allowing more than one or two layers to relax is significant for those surfaces which undergo large relaxations, which in Table I are the fcc (110) and the bcc (100) faces (these are the least densely packed faces). Inspection of the layer-by-layer displacements for these surfaces reveals that allowing more layers to relax does not merely give nonzero values for the displacements of the deeper planes, but also modifies the displacements of previously considered layers. For these faces, 3–6 layers participate in the relaxation as compared to 1–3 layers for the other faces. A tendency of the displacements to alternate in sign is noted, although for Na(111), for example, all layers relax outward. In general, after the first one or two layers, the magnitude of the relaxation decreases exponentially as one goes into the solid from the surface. In Table I and elsewhere, we use values

TABLE I. Relaxation of the spacing between the first and second layers, $\Delta_{12} = [\Delta(1) - \Delta(2)]/d$, in % (− denotes a contraction and + an expansion), and layer by layer displacements for the low-index faces of Al and Na using the exponential electron density, with values for the variational parameters β of 1.24 and 1.27 (a.u.)$^{-1}$, respectively, from Ref. 12. The integer L denotes the number of planes allowed to relax. The numbers in the fourth column are the values obtained for $\Delta(n)/a$, where $n = 0, 1, \cdots$ is the layer index.

Surface	L	Δ_{12} (%)	$\Delta(n)/a$
Al(100)	1	−1.1	−0.0054
	10	−1.2	−0.0054, 0.0008, −0.0001
Al(110)	1	−8.7	−0.0309
	2	−18.2	−0.0397, 0.0248
	5	−21.2	−0.0435, 0.0316, −0.0148, 0.0080, −0.0035
	10	−21.3	−0.0436, 0.0318, −0.0151, 0.0086, −0.0045
Al(111)	1	+0.6	+0.0036
	10	+0.6	+0.0036, 0.000 01
Na(100)	1	−6.3	−0.0317
	2	−9.5	−0.0349, 0.0127
	5	−9.9	−0.0353, 0.0139, −0.0044, 0.0015, −0.0004
	10	−9.9	−0.0353, 0.0139, −0.0044, 0.0015, −0.0005
Na(110)	1	−0.6	−0.0043
	10	−0.7	−0.0043, 0.0003
Na(111)	1	+3.7	+0.0108
	2	+3.6	+0.0108, 0.0003
	10	+3.6	+0.0108, 0.0003, 0.0001

for β taken from Smith.[12] We have repeated all exponential density calculations using β values given in the more recent work of Ma and Sahni,[18] and found qualitatively similar results.

The possibility that a number of layers may participate in the relaxation is potentially significant for LEED model calculations of scattered electron intensity versus incident energy (IV) profiles. In most LEED analyses of clean metal surfaces, only the top layer of ions has been allowed to relax in attempting to fit the experimental data. In a recent study of Cu(110) LEED intensity spectra, it was found that the structural model which fit the data best is an ~10% contraction of the first-second layer spacing, accompanied by perhaps a slight contraction or expansion between the second and third layers.[19] Similarly, for the Re(10$\bar{1}$0) surface, about a 17% contraction of the first-second layer distance and a modest expansion between the second and third layers appear to give the best agreement with experiment.[20] In light of these recent studies and our results it is suggested that multilayer relaxation models be considered more routinely in LEED analyses and in the interpretation of ion scattering and channeling experiments.

Table II illustrates the dependence of the relaxation upon the model used for the electron charge density. The step-function density yields contractions for all of the faces studied. The exponential density profile produces smaller contractions than the step-function density for the (001) and (110) faces, and predicts expansion of the first-second layer distance for the (111) faces of all three materials. With the Lang-Kohn densities, the calculated relaxations are generally of the same sign as the exponential density results, but in some cases are significantly different in size. The charge density dependence of the relaxation appears to be stronger for the higher r_s-value materials. This can be rationalized by considering the Lang-Kohn charge densities for Al, Li,

TABLE II. Relaxation of the first-second and second-third layer spacings Δ_{12} and Δ_{23}, $\Delta_{mn} = [\Delta(m) - \Delta(n)]/d$, for the low-index faces of Al, Li, and Na using three models for the charge density: (a) step-terminating, (b) exponential, and (c) Lang-Kohn. Values for Δ_{12} and Δ_{13} are given in percent. For the exponential density profile results, the parameter β was taken to be 1.24, 1.24, and 1.27 (a.u.)$^{-1}$ for Al, Li, and Na, respectively. Ten layers were allowed to relax for all results listed.

	Step		Exponential		Lang-Kohn	
Surface	Δ_{12}	Δ_{23}	Δ_{12}	Δ_{23}	Δ_{12}	Δ_{23}
Al(100)	−2.4	0.3	−1.2	0.2	−2.0	0.4
Al(100)	−26.3	15.8	−21.3	13.3	−23.9	14.4
Al(111)	0.0	0.0	+0.6	0.0	+0.3	0.0
Li(100)	−10.9	4.0	−8.7	3.3	−16.3	7.4
Li(110)	−0.9	0.1	−0.3	0.0	−2.0	−0.4
Li(111)	−0.9	0.0	+6.7	0.3	+9.0	−3.1
Na(100)	−10.9	4.0	−9.9	3.7	−20.3	9.4
Na(110)	−0.9	0.1	−0.7	0.0	−2.6	−0.6
Na(111)	−0.9	0.0	+3.6	0.1	+4.0	−4.1

and Na, which are shown in Fig. 2; the Li density was obtained via a six-point, two-dimensional interpolation of the charge densities given in Table I of Ref. 13. As seen in the figure, the Friedel oscillations at the surface of Al ($r_s = 2.0$) are much smaller than for the higher r_s materials. In an electrostatic force model, such differences in negative charge accumulations can have a significant effect on the results. As noted by Alldredge and Kleinman (AK),[10] this may account for the apparent success of the calculation by FH[8] for Al, where a step-function density was assumed.

The effect of pseudopotential corrections is shown in Table III. Both Ashcroft (empty core)[17,21] and simplified Heine-Abarenkov pseudopotentials[16] have been employed in conjunction with the exponential density profiles. The pseudopotential corrections lead to substantial changes in the relaxations calculated, and generally tend to favor expansion, or equivalently, to reduce contraction. Plausible variations in the pseudopotential parameters produce modest but in some cases non-negligible changes. Unrealistically large expansions are predicted for the bcc (111) faces; these are the only cases treated for which the Ashcroft pseudopotential cores for atoms in the first layer extend well beyond the plane at $\frac{1}{2}d$.

In Table IV, we compare our results for Al, Li, and Na with available previous studies,[1,8,10,22,23] including LEED analyses. For the step-function density there are substantial differences between the one-layer relaxation results and those obtained with the original FH model,[8] which considered only the interaction of a surface ion with the smoothed electron density in its own surface Wigner-Seitz cell. Further changes are evident when more layers are allowed to relax. Using a one-layer relaxation model, AK[10] have emphasized the importance of crystalline effects in their study of the Li(100) surface. They conclude that the Lang-Kohn density yields an electrostatic force on the first layer of about one fourth of the total crystalline result. Table IV shows again that multilayer relaxation mechanisms, electron density variations and pseudopotential corrections all can produce large changes comparable in magnitude to other crystalline effects. Our electrostatic model is sufficiently simple that we do not want to belabor

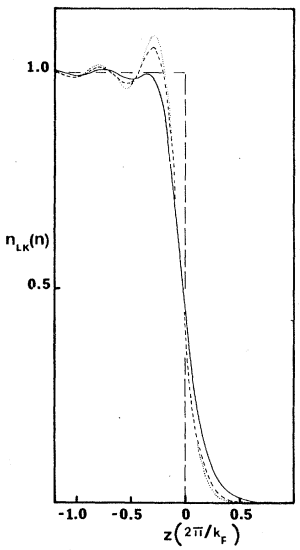

FIG. 2. Lang-Kohn charge densities derived for a uniform jellium model (after Ref. 15), for $r_s = 2.0$, 3.25, and 4.0, solid, dashed, and dotted curves, respectively. The coordinate z is in units of the Fermi wavelength, and the densities n_{LK} in units of the bulk density $n_0 = ze/Ad$. To agree with our convention that the first ion layer is located at $z = 0$, the coordinates in this figure are to be shifted by $(+\, d/2)$, where d is the layer spacing in the unrelaxed lattice.

TABLE III. The effect of pseudopotential correction on relaxation of the first-second layer spacing Δ_{12} for the low-index faces of Al, Li, and Na. Values for Δ_{12} are given as a percentage of the bulk interlayer spacing d. The first column in the top half of the table, labeled None, gives the results obtained with the exponential charge density profile and no pseudopotential corrections. The next four columns, labeled Al, A2, HA1 and HA2, list values obtained using the exponential density and two Ashcroft and two simplified Heine-Abarenkov pseudopotentials The pseudopotential radii and well-depth parameters for the four models are given (in atomic units) in the lower half of the table. Values used for β were 1.24, 1.24, and 1.27 (a.u.)$^{-1}$ for Al, Li and Na, respectively, and ten layers were allowed to relax in the calculations.

Surface	None	Al[a]	A2[b]	HA1[c]	HA2[d]
Al(100)	−1.2	+0.2	+0.2	+0.1	+0.5
Al(110)	−21.3	−14.5	−14.7	−15.2	−13.1
Al(111)	+0.6	+1.4	+1.4	+1.3	+1.5
Li(100)	−8.7	+0.1	−6.2	−4.6	−3.8
Li(110)	−0.3	+1.4	+0.2	+0.4	+0.6
Li(111)	+6.7	+41.0	+18.7	+23.5	+24.8
Na(100)	−9.9	−5.5	−6.2	−6.0	−3.7
Na(110)	−0.7	+0.1	0.0	−0.1	+0.5
Na(111)	+3.6	+29.8	+26.7	+21.7	+26.1

	Al		Li		Na	
	r_0	a_0	r_0	a_0	r_0	a_0
A1	1.131	∞	1.678	∞	1.758	∞
A2	1.12	∞	1.06	∞	1.66	∞
HA1	2.0	1.82	2.8	2.32	3.4	2.87
HA2	2.0	1.99	2.8	2.38	3.4	3.11

[a] Reference 21.
[b] Table XV of Ref. 17.
[c] Table 8-3 of Ref. 16; $Z/a_0 = (A_0 + A_1 + A_2)/3$.
[d] Table 8-3 of Ref. 16; $Z/a_0 = (A_0 + A_1)/2$.

TABLE IV. Comparison of results obtained for the relaxation of the first-second layer distance Δ_{12} for Al, Li, and Na surfaces. Values for Δ_{12} are given as percentages of the bulk interlayer spacing d. The columns labeled FH, AK, and TF give values for Δ_{12} taken from Refs. 8, 10, and 22, respectively. For the present calculations, the columns labeled a, b, b′, and c indicate that the following charge densities were used: (a) step function, (b) exponential, β as in Table II, (b′) exponential, β as in Table II, with Ashcroft pseudopotential corrections (A2 in Table II), and (c) Lang-Kohn. The LEED results in the last column are taken from a recent compilation in Table 2 of Ref 1.

				Present calculation								
				1 layer				10 layers				
	FH	AK	TF	a	b	b′	c	a	b	b′	c	LEED
Al(100)	−4.6	···		−2.1	−1.1	+0.2	−1.6	−2.4	−1.2	+0.2	−2.0	0
Al(110)	−16.0	···	+2.0	−11.4	−8.7	−5.0	−10.2	−26.3	−21.3	−14.7	−23.9	−5 ~ −15
Al(111)	−1.6	···	0.0	0.0	+0.6	+1.4	+0.4	0.0	+0.6	+1.4	+0.3	+2.5
Li(100)	−10.4[a]	−20.0	···	−7.0	−5.5	−3.8	−9.0	−10.9	−8.7	−6.2	−16.3	···
Na(110)	···	···	···	−0.8	−0.6	0.0	−3.1	−0.9	−0.7	0.0	−2.6	0

[a] FH model value given in Ref. 10 (AK).

comparisons with experimentally derived numbers, but we do want to point out that the ten-layer relaxation results are in good qualitative agreement with LEED analysis, particularly for the exponential density with pseudopotential corrections.

Table V presents some results for the low-index faces of Cu. Ma *et al.*[11] have investigated the Cu(100) surface using a combination of empirical pair potentials and electrostatic forces for a step-function electron density, and predicted a 0.5% expansion of the first-second layer spacing. Our calculations give small contractions or expansions for the (100) face depending on the model and the parameter values employed. LEED analysis for Cu(100) indicates that very little relaxation occurs.[24] For the (110) face, our results show a sizable contraction in the first-second layer distance. This can be brought into agreement with the most recent LEED analysis[19] by varying the exponential charge density parameter β (row 3 in Table V), but the 9% expansion of the second-third layer spacing that is then calculated is much larger than the ±2.5% determined from the LEED data.

TABLE V. Relaxation of the first-second and second-third layer spacings Δ_{12} and Δ_{13}, in percent of the bulk interlayer spacing d, for the low-index faces of Cu. Results are given for five model calculations, as indicated in the first column: step-function density, exponential density profile with two values for β (in a.u.), exponential density profile with the same two values for β and pseudopotential corrections for an Ashcroft pseudopotential with $r_0 = 0.81$ a.u. (cf. Table XV of Ref. 17). Ten layers were allowed to relax in all of the calculations. The last row of the table gives LEED analysis results from Refs. 1, 19, and 24.

Model	(100)		(110)		(111)	
	Δ_{12}	Δ_{23}	Δ_{12}	Δ_{23}	Δ_{12}	Δ_{23}
Step	−2.4	0.3	−26.3	15.8	0.0	0.0
Exponential, $\beta = 1.23$	−0.7	0.1	−19.3	12.4	+0.9	0.0
Exponential, $\beta = 0.87$	+2.2	0.0	−10.2	9.0	+2.8	0.1
Ashcroft, $\beta = 1.23$	+0.3	0.0	−14.9	10.3	+1.5	0.0
Ashcroft, $\beta = 0.87$	+3.7	0.0	− 4.9	6.9	+3.7	0.1
LEED	~0		−10.0	±2.5	−4.0	

On the whole, we observe that our simple electrostatic model results give relaxation trends for the low-index faces of fcc and bcc *sp*-bonded metals that are qualitatively consistent with those obtained via analyses of diffraction data. We have demonstrated the importance of multilayer relaxation mechanisms, charge density variations, and pseudopotential corrections. Particularly in view of these effects, several ways to improve the model are suggested. One would be to employ crystalline electronic charge densities with variations parallel as well as perpendicular to the surface, which would provide added sensitivity to the crystal face of the material under study.[10,25] A second, more difficult, but clearly important refinement would be to use self-consistent charge densities which are recalculated in each iteration in the adiabatic approximation. Another avenue of improvement would be to augment the model with short-range interactions.[11] As seen from Eq. (14), the coefficients $a_{ll'}$ can be regarded as static interplanar force constants that can be related to appropriate linear combinations of interatomic force constants.[26,27] From empirical fits of the latter to the phonon dispersion curves, an estimate of the additional short-range interactions might be obtained. We are working at present to incorporate these modifications.

TABLE VI. Crystallographic relationships for the low-index faces of cubic structures. (See Appendix B for notation.)

Crystal face	$\vec{a}_1$	$\vec{a}_2$	$\vec{b}_1$	$\vec{b}_2$	A	B	d	n_0	$P_G(n)$
fcc (001)	$(a/2)(1\bar{1}0)$	$(a/2)(110)$	$(2\pi/a)\ (1\bar{1}0)$	$(2\pi/a)\ (110)$	$a^2/2$	$2(2\pi/a)^2$	$a/2$	2	$P_G(2l+1)=1,\ P_G(2l+2)=(-1)^{\mu+\nu}$
fcc (110)	$a(001)$	$(a/2)(1\bar{1}0)$	$(2\pi/a)\ (001)$	$(2\pi/a)\ (1\bar{1}0)$	$a^2/\sqrt{2}$	$\sqrt{2}(2\pi/a)^2$	$a/2\sqrt{2}$	2	$P_G(2l+1)=1,\ P_G(2l+2)=(-1)^{\mu+\nu}$
fcc (111)	$(a/2)(\bar{1}10)$	$(a/2)(0\bar{1}1)$	$(4\pi/3a)(\bar{2}11)$	$(4\pi/3a)(\bar{1}\bar{1}2)$	$\sqrt{3a^2}/4$	$(4/\sqrt{3})(2\pi/a)^2$	$a/\sqrt{3}$	3	$P_G(2l+1)=1,\ P_G(2l+2)=e^{i(2\pi/3)(\mu+\nu)},$ $P_G(2l+3)=e^{i(4\pi/3)(\mu+\nu)}$
bcc (001)	$a(100)$	$a(010)$	$(2\pi/a)\ (100)$	$(2\pi/a)\ (010)$	a^2	$(2\pi/a)^2$	$a/2$	2	$P_G(2l+1)=1,\ P_G(2l+2)=(-1)^{\mu+\nu}$
bcc (110)	$a(001)$	$(a/2)(1\bar{1}\bar{1})$	$(\pi/a)\ \ (1\bar{1}2)$	$(2\pi/a)\ (1\bar{1}0)$	$a^2/\sqrt{2}$	$\sqrt{2}(2\pi/a)^2$	$a/\sqrt{2}$	2	$P_G(2l+1)=1,\ P_G(2l+2)=(-1)^{\mu}$
bcc (111)	$(a/2)(\bar{1}10)$	$(a/2)(0\bar{1}1)$	$(4\pi/3a)(\bar{2}11)$	$(4\pi/3a)(\bar{1}\bar{1}2)$	$\sqrt{3a^2}/4$	$(4/\sqrt{3})(2\pi/a)^2$	$a/2\sqrt{3}$	3	$P_G(2l+1)=1,\ P_G(2l+2)=e^{i(4\pi/3)(\mu+\nu)}$ $P_G(2l+3)=e^{i(4\pi/3)(\mu+\nu)}$

ACKNOWLEDGMENTS

The authors are grateful to Mark Rasolt and L. H. Jenkins for critical comments on the manuscript. This work was supported by the U. S. DOE under Contract No. EG-77-S-05-5489 and by the Division of Materials Science, U. S. DOE under Contract No. W-7405-eng-26 with the Union Carbide Corporation.

APPENDIX A

The derivation of the electrostatic forces presented in Sec. II for the fcc (100) and (110) faces and the bcc (100) face is extended in this Appendix to the (111) faces of these cubic structures. Following the steps leading to Eq. (9), we obtain for the forces on ions in the mth layer due to those in the nth layer an identical expression, but with $P_{\vec{G}}(n)$ defined as (see Appendix B)

$$P_{\vec{G}}(n)=\exp[2\pi i(\mu+\nu)\bmod(n,3)/3]\,, \tag{A1}$$

where the $\mathrm{mod}(a,b)$ function is defined as

$$\mathrm{mod}(a,b)=a-[a/b]b\,,$$

and $[x]$ is the largest integer which does not exceed x. For the expression for F_m corresponding to Eq. (12), we obtain

$$F_m=\sum_{\vec{G}}\frac{e^{-Gd}}{1-e^{-3Gd}}(1+X+X^2)P_{\vec{G}}(L+1)\times P^{*}_{\vec{G}}(m)e^{-G[(L-m)d-\Delta(m)]}\,, \tag{A2}$$

where

$$X=\exp[-Gd+(2\pi i/3)(\mu+\nu)]\,. \tag{A3}$$

APPENDIX B

In this Appendix we compile crystallographical relationships for the low-index faces of cubic structures. The following notations are used:

$\vec{a}_1, \vec{a}_2$ are the primitive real-mesh translation vectors.

$\vec{b}_1, \vec{b}_2$ are the primitive reciprocal-mesh vectors; $\vec{a}_i\cdot\vec{b}_j=2\pi\delta_{ij}$.

$\vec{G}=\mu\vec{b}_1+\nu\vec{b}_2$ is the reciprocal-mesh vector.

A, B are real and reciprocal unit mesh areas.

d is the interlayer spacing in the unrelaxed real lattice.

n_0 is the repeat sequence for planes, i.e., plane $n+n_0$ has the same origin as plane n (in $2D$).

$P_{\vec{G}}(n)=\exp -i\vec{G}\cdot\vec{R}_n$ is the phase function for plane n. The indexing of planes is $n=0,1,\ldots,$ with $n=0$ being the top-most surface plane.

Table VI lists the above for the various fcc and bcc faces.

[1]F. Jona, J. Phys. C: Solid State Phys. 11, 4271 (1978).
[2]E. G. McRae and H. D. Hagstrum, in *Treatise on Solid State Chemistry*, edited by N. B. Hannay (Plenum, New York, 1976), Vol. 6A(I), Chap. 2.
[3]D. P. Jackson, Can. J. Phys. 49, 2093 (1971).
[4]S. Kato, Jpn. J. Appl. Phys. 13, 218 (1974).
[5]J. W. Flocken, Phys. Rev. B 9, 5133 (1974).
[6]R. A. Johnson and P. J. White, Phys. Rev. B 13, 5293 (1976).
[7]R. Benedek, J. Phys. F 8, 1119 (1978).
[8]M. W. Finnis and V. Heine, J. Phys. F 4, L37 (1974).
[9]R. Smoluchowski, Phys. Rev. 60, 661 (1941).
[10]G. P. Alldredge and L. Kleinman, Phys. Lett. 48A, 37 (1974); J. Phys. F 4, L207 (1974); G. P. Alldredge, in *Computer Simulation for Materials Applications*, Nuclear Metallurgy, edited by R. J. Arsenault, J. R. Beeler, Jr., and J. A. Simmons (NBS, Washington, D.C., 1976), Vol. 20, p. 582.
[11]S. K. S. Ma, F. W. de Wette, and G. P. Alldredge, Surface Sci. 78, 598 (1978); G. P. Alldredge and S. K. S. Ma, Phys. Lett. 51A, 155 (1975).
[12]J. R. Smith, Phys. Rev. 181, 522 (1969).
[13]N. D. Lang and W. Kohn, Phys. Rev. B 1, 4555 (1970).
[14]C. A. Sholl, Proc. Phys. Soc. 91, 434 (1967); F. W. de Wette and G. E. Schacher, Phys. Rev. 137, A78, A92 (1965).
[15]I. V. Abarenkov and V. Heine, Phil. Mag. 12, 529 (1965).
[16]W. A. Harrison, *Psuedopotentials in the Theory of Metals* (Benjamin, New York, 1966).
[17]M. L. Cohen and V. Heine, in *Solid State Physics*, edited by F. Seitz, D. Turnbull, and H. Ehrenreich (Academic, New York, 1970), p. 37.
[18]C. Q. Ma and V. Sahni, Phys. Rev. B 19, 1290 (1979).
[19]H. L. Davis, J. R. Noonan, and L. H. Jenkins, Surface Sci. 83, 559 (1979).
[20]H. L. Davis and D. M. Zehner, J. Vac. Sci. Technol. (to be published).
[21]F. Perrot, Phys. Status Solidi B 81, 205 (1977).
[22]C. Tejedor and F. Flores, J. Phys. F 6, 1647 (1976).
[23]We note that in Ref. 13, Appendix E, a calculation in which the topmost layer of ions at the (111) face of an fcc structure was allowed to shift from its truncated bulk position yielded an expansion $\Delta_{12} = 0.5\%$ for aluminum.
[24]J. R. Noonan and H. L. Davis, J. Vac. Sci. Technol. (to be published); D. L. Adams and U. Landman, Phys. Rev. B 15, 3775 (1977).
[25]R. Monnier, J. P. Perdew, D. C. Langreth, and J. W. Wilkins, Phys. Rev. B 18, 656 (1978).
[26]A. J. E. Foreman and W. M. Lomer, Proc. Phys. Soc. London Sec. B 70, 1143 (1957).
[27]B. N. Brockhouse, T. Arase, G. Caglioti, K. R. Rao, and A. D. B. Woods, Phys. Rev. 128, 1099 (1962).